2

Neutrino Physics

Contents

Despite being one of the most abundant particle in the universe, neutrinos are some of the most elusive; due to the fact that neutrinos can only interact via the weak interaction. The history of neutrino physics is therefore strongly connected to the discovery and study of weak interactions. Measurements by Chadwick in 1914 showed that the energy spectrum of electrons released in (β–decays was continuous, this is in contrast to discrete spectra observed in α and γ decays, and seemingly violates conservation of energy under the assumption of a two–body final state which was expected at the time. In order to solve this problem, Pauli postulated that the continuous energy spectrum could be explained if the energy

released in a β–decay could be shared with an additional neutral weakly interacting fermion which Pauli named the neutron. Fermi later renamed Pauli's fermion to the neutrino after Chadwick discovered the neutron in 1932. Despite claims that neutrinos might never be detected, neutrinos have now been discovered and they have been found to have a number of interesting properties which were not anticipated when neutrinos were first postulated. This chapter will detail some of the history and theory of neutrino's and their interactions.

In this chapter, Section 2.1 will give a brief historical overview of neutrino physics. Section 2.2 will introduce the theory of neutrinos in the Standard Model, followed by a discussion of neutrino oscillations in Section 2.3. Neutrino interactions will be discussed briefly in Section 2.4. Finally Section 2.5 will discuss the production and measurement of neutrinos from supernovae.

2.1 A Brief History of Neutrino Physics

The first attempt to incorporate the neutrino into a theoretical model came in 1934 when Fermi presented his theory of β–decay, in this theory the neutrino takes part in a four–point interaction with the other components of the β–decay interaction [10]. The incredible success of this theory in explaining the observed properties of β–decays provided strong evidence for the neutrinos existence, however, in 1934 after using Fermi's theory to predict the strength of neutrino interactions, H. Bethe and R. Peierls found that the interactions were so weak that they might never be observed, a prediction that held true for over 20 years [11].

The first breakthrough in experimental neutrino physics would come in 1956. F. Reines and C. Cowan were attempting to measure positrons produced in inverse β–decay interactions,

$$\overline{\nu_e} + p \rightarrow n + e^+. \tag{2.1}$$

A detector containing 1400 litres of liquid scintillator was used to measure the large flux of electron anti–neutrinos in the vicinity of the Savannah River nuclear reactor. They observed a large increase in the rate of positron events when the reactor

was on compared to when the reactor was switched off, the first experimental evidence for the existence of neutrinos [12].

The discovery of the electron neutrino opened the door to answer questions of neutrino flavour. As neutrinos are produced alongside a charged lepton it is natural to compare the properties of neutrinos with their partners in the weak interaction. At the time of the discovery of the neutrino there were two known charged leptons, the electron and the muon, and physicists asked whether the neutrinos produced alongside muons are different from those produced alongside electrons. In 1962, Lederman et al discovered the muon neutrino at Brookhaven National Laboratory; by creating a beam of muon–associated neutrinos from decaying pions, and observing the leptons produced in neutrino interactions after all other particles had been absorbed. They found that only muons where produced in the resulting neutrino interactions, and therefore the neutrinos produced were only ever associated with a muon, which shows that neutrinos are produced with a distinct flavour in weak interactions [13].

In 1973 the Gargamelle experiment at CERN released results on the measurement of neutrino interactions [14]. They observed a new type of interaction, neutral current (NC) interactions:

$$\nu_l + N \rightarrow \nu_l + X \tag{2.2}$$

which are characterised by the lack of an observable charged lepton in the final state. Unlike charged current (CC) interactions, which are mediated by the charged W boson, these NC interactions are mediated by the neutral Z^0 boson.

With the discovery of the tau–lepton in 1977 it was expected that there should be an associated tau neutrino, however, it wouldn't be detected until 2001 by the DONUT experiment [15]. In the experiment, tau neutrinos where produced from the decay of charmed mesons produced in collisions between protons and a stationary target. The neutrino interactions where detected in emulsion detectors, where the unique geometry of the interaction, in which a short tau track is produced

at the vertex followed by a long muon track, allowed them to be distinguished from other decays.

While additional neutrino species are possible, data from measurements of the Z boson line–shape at LEP in 1992 restricts the number of active light neutrino species to be three [16]. An active light neutrino is any neutrino with $m_\nu < \frac{m_Z}{2}$ that can interact with the Z boson, such that the decay $Z \to \nu\nu$ is possible.

Alongside the discovery of three different types of neutrino, there were interesting results when observing neutrinos produced in the Sun. The flux of neutrinos from the Sun at the earth surface had been predicted with Bachall's Standard Solar Model (SSM), however, in 1968 when Davis et al measured the flux in the Homestake experiment they found a deficit with respect to the prediction of the SSM [17, 18], the so called solar neutrino problem. In the Homestake experiment electron neutrinos where being measured via there inverse beta decay interactions with the chlorine in the target,

$$v_e + {}^{37}\mathrm{Cl} \to {}^{37}\mathrm{Ar} + e^-. \tag{2.3}$$

The neutrino interaction rate was measured by counting the number of argon atoms in the chlorine tank by capturing them on helium gas which was periodically bubbled through the chamber.

In addition to the solar neutrino problem, a similar deficit was observed in 1988 for muon neutrinos produced during cosmic ray showers. The Kamiokande experiment was able to measure both electron and muon neutrino interactions via the cerenkov radiation produced by the charged leptons in water. Their data was consistent with the expected rate of electron neutrinos from the atmosphere, however, a deficit of muon neutrinos was observed [19].

The next generation of the Kamiokande experiment, Super–Kamiokande, aimed to understand the observed deficit of atmospheric muon neutrinos with a larger water cerenkov detector capable of resolving the angular distribution of atmospheric neutrino interactions. Super–Kamiokande consists of a cylindrical vessel containing 50 kt of ultra pure water, surrounded by an array of around 13,000 photomultiplier

tubes to detect the cerenkov light. Electron and muon neutrinos can be distinguished based on the pattern of cerenkov light that is left in the detector; muons leave clear cerenkov rings in the detector due to their higher mass while electrons, which can scatter and shower, tend to leave diffuse "fuzzy" rings on the wall of the detector. In 1998, Super–Kamiokande published measurements of the flux of atmospheric muon neutrinos as a function of azimuthal angle [20]. Since these neutrinos are created a short distance from the earths surface, the incoming angle of the neutrino can be used to estimate the distance travelled by the neutrino before arriving at the detector; the down–going neutrinos have only travelled a short distance in the atmosphere ($\sim$ 10km), while the up–going neutrinos have travelled through the entire earth to reach the detector ($\sim 13,000$km). Figure 2.1, shows the flux of neutrinos measured by Super Kamiokande as a function of L/E_ν; the muon neutrino flux is consistent with the no oscillation prediction at small L/E_ν, however, for large L/E_ν a clear deficit is observed.

While it wouldn't completely solve the solar neutrino problem, the Sudbury Neutrino Observatory (SNO) was able to provide unique insight into the observed solar neutrino fluxes in 2002. Unlike other water cerenkov detectors, SNO was filled with heavy water, D_2O, instead of its lighter isotope. The use of heavy water gives rise to additional neutrino interactions which allowed the SNO experiment to distinguish between three different interaction modes: charged current (CC), neutral current (NC), and elastic scattering (ES). Each mode is sensitive to different parts of the solar neutrino flux, including some sensitivity to the muon neutrino and tau neutrino fluxes via the NC and ES interactions. Analysis of the data for each of the three unique interaction modes lead to a measurement of the flavour composition of the solar neutrino flux at earth, while also finding the overall neutrino flux at earth to be consistent with the SSM. Figure 2.2 shows the composition of the solar neutrino flux as measured in the SNO experiment [21], the flux prediction based on the measured rate of NC events is consistent with the predictions of the SSM. The composition of solar neutrinos measured in the SNO experiment is not a result of neutrino oscillations, instead it is the result of the effect of matter

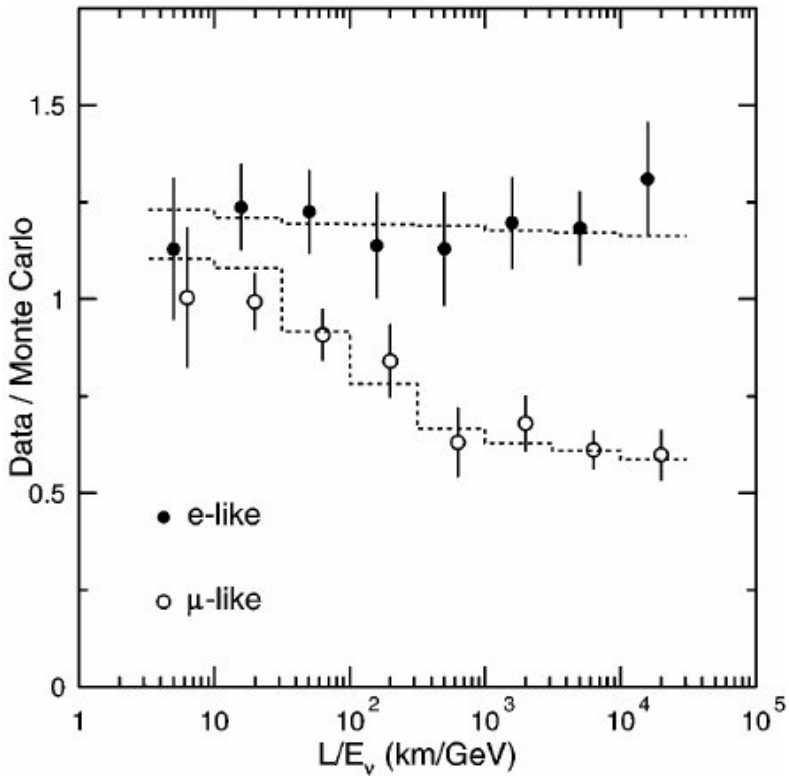

Figure 2.1: Ratio of data to Monte Carlo for electron and muon neutrino fluxes measured by the Super Kamiokande experiment as a function of L/E_ν. The Monte Carlo prediction is based on the assumption of no oscillations. The muon neutrino flux is consistent with the no oscillation prediction at small L/E_ν, however, for large L/E_ν a clear deficit is observed. The best fit under the assumption of atmospheric ($\nu_\mu \rightarrow \nu_\tau$) oscillations is shown, the best fit parameters are $\Delta m^2 = 2.2 \times 10^{-3}\text{eV}^2$, and $\sin^2 2\theta = 1$. [20].

on the neutrino propagation in the Sun via the Mikheyev–Smirnov–Wolfenstein (MSW) effect. However at the time a number of solutions were still possible: MSW conversion, decoherence, neutrino decay, and others [22].

An L/E_ν dependence in the neutrino flux would have to be measured in order for neutrino oscillations to be the unique solution to the problem. To make this measurement a much shorter neutrino baseline would be needed, along with a source of neutrinos with a small energy spread, and a detector with good energy resolution. In 2002 the Kamioka Liquid Scintillator Anti–neutrino Detector (KamLAND) experiment measured $\overline{\nu_e}$ oscillations from a number of nuclear reactors, which produce neutrinos at the MeV scale [23, 24]. Along with an overall deficit of neutrino events, they were able to use the high energy resolution of the KamLAND detector to measure an L/E_ν dependence of the $\overline{\nu_e}$ survival probability. Figure 2.3,

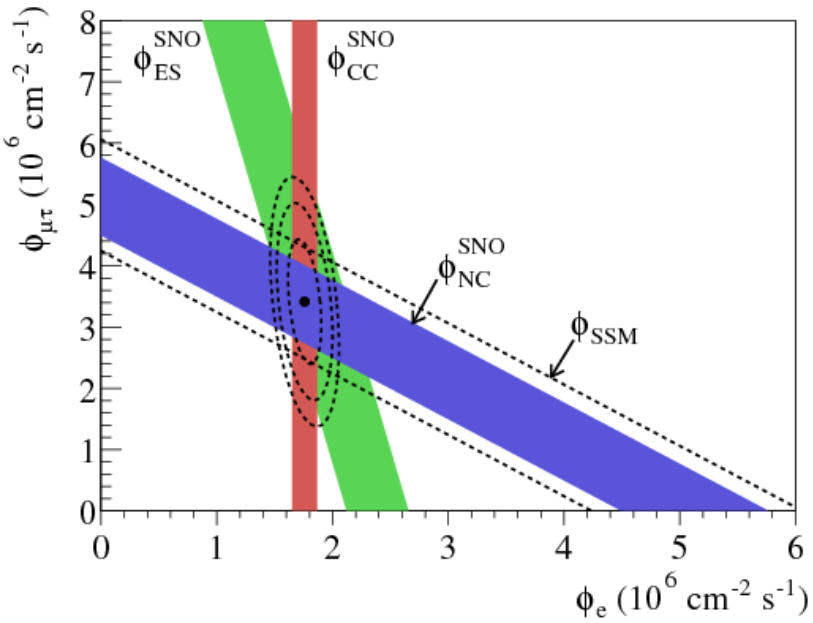

Figure 2.2: Solar neutrino flux composition as measured by the SNO experiment. The coloured bands represent the measured flux of charged current (CC), neutral current (NC), and elastic scattering (ES) events, including a $\pm 1\sigma$ spread. The central contours represent 68%, 95%, and 99% probability contours for the joint ϕ_e and $\phi_{\mu\tau}$ fit. The dashed lines represent the predicted flux of ^{8}B neutrinos based on the standard solar model [21].

shows the ratio of the observed neutrino flux with the no oscillation predicted flux as a function of L/E_ν, a clear dependence can be seen and this data was enough to prove that neutrino oscillations were the only solution to the solar neutrino problem.

Based on the results of the above experiments, it was assumed that electron and muon type neutrinos where oscillating into tau type neutrinos which where then left undetected. The first evidence of tau neutrino production in oscillations wouldn't come until 2010, when the OPERA experiment measure a ν_τ candidate in a ν_μ beam. They used similar emulsion detectors to those used to discover the ν_τ in DONUT, and a muon neutrino beam on a 730km baseline from CERN to LNGS. By the end of the experiment a total of 10 candidate events have been observed, 6.1 σ above the expected background [25, 26].

Since the discovery of neutrino oscillations, many more experiments have made measurements of oscillations and the majority of the parameters of the neutrino oscillation models have been constrained. Important results of these experiments for

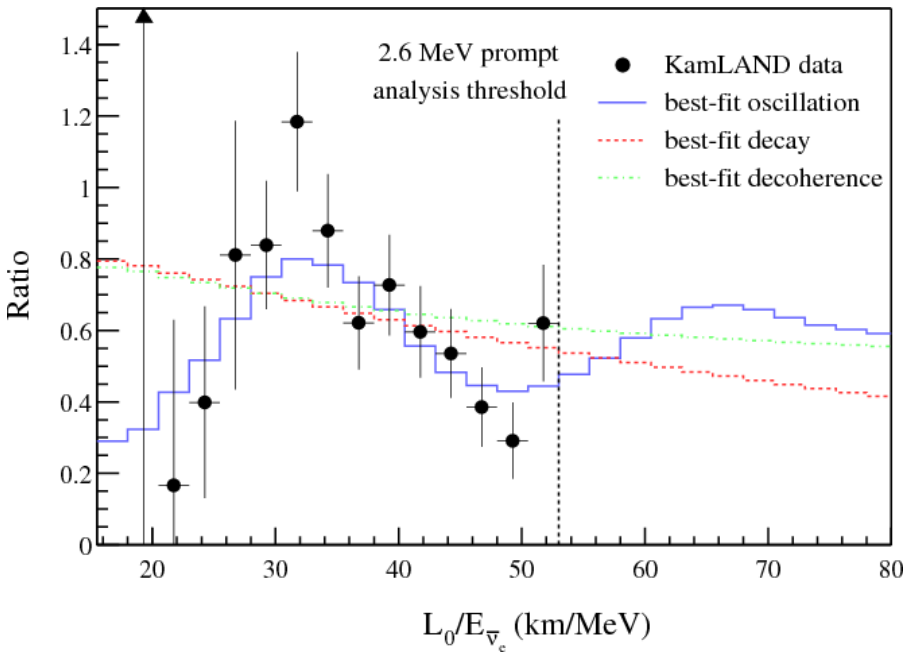

Figure 2.3: Ratio of observed neutrino flux to the predicted flux in the absence of neutrino oscillations in the KamLAND experiment as a function of L/E_ν. The data are fit with three different models: the red dashed line represents the best fit to a neutrino decay model, the green dashed line is for a decoherence model, and the solid blue line represents the best fit of the data to a neutrino oscillation model. The neutrino oscillation model, which has a different shape to the other two models, is found to give the best fit to the data [24].

constraining the parameters of the neutrino oscillation models will be highlighted in Section 2.3, along with a theoretical overview of neutrino oscillations.

Neutrino oscillations are currently the only measured effect that is not explained in the SM, and their observation proves that neutrinos are massive. However, the absolute mass of neutrinos is still unknown. The question of absolute neutrino mass, is one of a number of open questions in neutrino physics. At the time of writing, the main open questions in neutrino physics are:

- What are the absolute masses of the neutrinos?
- What is the mass ordering of the neutrino mass eigenstates?
- Is there CP violation in the neutrino sector?
- Are neutrinos Dirac ($\nu \neq \bar{\nu}$) or Majorana ($\nu = \bar{\nu}$) particles?

2.2 Neutrinos in the Standard Model

In the standard model neutrinos form part of the left handed fermion doublets

$$\psi_i = \begin{pmatrix} \nu_i \\ l_i^- \end{pmatrix}, \tag{2.4}$$

where they are paired with a charged lepton of the same flavour in CC interactions, and i represents any of the three known generations of leptons. Their interactions with other particles in the standard model is determined by the electroweak (EW) theory, which is derived from the $SU(2) \times U(1)$ gauge group. The neutrino fields enter into the SM Lagrangian in the CC and NC interactions:

$$\mathcal{L}^{CC} = -\frac{g_W}{2\sqrt{2}}\, j_\alpha^{CC}(x)\, W^\alpha(x) \;+\; h.c. \tag{2.5}$$

$$\mathcal{L}^{NC} = -\frac{g_W}{2cos\theta_W}\, j_\alpha^{NC}(x)\, Z^\alpha(x) \;+\; h.c. \tag{2.6}$$

Here

$$j_\alpha^{CC}(x) = 2 \sum_{\beta=e,\mu,\tau} \overline{\nu_\beta}(x)\, \gamma_\alpha\, l_\beta(x) \tag{2.7}$$

is the leptonic charged–current and

$$j_\alpha^{NC}(x) = \sum_{\beta=e,\mu,\tau} \overline{\nu_\beta}(x)\, \gamma_\alpha\, \nu_\beta(x) \tag{2.8}$$

is the neutrino neutral–current, $W^\alpha(x)$ and $Z^\alpha(x)$ are the vector boson fields for the $W^\pm$ and Z^0 bosons respectively, g_W is the electroweak coupling constant, and θ_W is the Weinberg angle.

Mass is included in the standard model through the Dirac mass term in the Lagrangian

$$\begin{aligned} \mathcal{L}^D &= m_D \overline{\psi}\psi \\ &= m_D \overline{(\psi_L + \psi_R)}(\psi_L + \psi_R) \\ &= m_D(\overline{\psi}_L\psi_R + \overline{\psi}_R\psi_L) \end{aligned} \tag{2.9}$$

where L and R represent the left and right handed components of the field. The lack of right handed neutrino states therefore means neutrinos are assumed to

be massless in the standard model. For massive neutrinos to exists the standard model, right handed neutrino fields need to be introduced. In addition, it is still not whether neutrinos are Dirac or Majorana particles, meaning that additional Majorana mass terms are possible. A more general neutrino mass term including both Dirac and Majorana components is

$$\mathcal{L}^{D+M} = \begin{pmatrix} \bar{\nu}_L & \bar{\nu}_R \end{pmatrix} \begin{pmatrix} m_L & m_D \\ m_D & m_R \end{pmatrix} \begin{pmatrix} \nu_L \\ \nu_R \end{pmatrix}. \tag{2.10}$$

2.3 Neutrino Oscillations

Neutrino oscillations are a result of quantum mechanical interference between different massive neutrino eigenstates. The mass eigenstates are produced and measured coherently because the energy and momenta of the neutrino states are not measured with enough precision to distinguish the mass eigenstate of the neutrino.

Neutrinos are produced in a state of definite flavour, $\alpha = e, \mu, \tau$, in charged current (CC) and neutral current (NC) weak interactions,

$$W^+ \to l_\alpha^+ \nu_\alpha, \quad W^- \to l_\alpha^- \nu_\alpha, \quad Z \to \nu_\alpha \overline{\nu_\alpha}. \tag{2.11}$$

The CC processes are used in neutrino oscillation experiments because they give information about the initial flavour state of the neutrinos. These processes are governed by the Lagrangian of the CC leptonic interactions, as in Equation 2.5.

Neutrino flavour states, ν_α, can be represented as a superposition of massive neutrinos in any case where the energy and momentum of the neutrino is not known with enough precision to determine the neutrino mass. The basis transformation takes the form

$$\nu_\alpha = \sum_k U_{\alpha k}^* \nu_k, \tag{2.12}$$

where ν_k are the neutrino mass eigenstates, and U is a unitary mixing matrix.

The representation of neutrino flavour states as a superposition of mass eigenstates gives rise to the phenomenon of neutrino oscillations. Consider a neutrino produced in a CC weak interaction with flavour α. This neutrino flavour state is

described by equation 2.12, where U is a unitary mixing matrix called the PMNS (Pontecorvo, Maki, Nakagawa, and Sakata) matrix. For three flavour mixing the PMNS matrix takes the form:

$$U = \begin{pmatrix} U_{e1} & U_{e2} & U_{e3} \\ U_{\mu 1} & U_{\mu 2} & U_{\mu 3} \\ U_{\tau 1} & U_{\tau 2} & U_{\tau 3} \end{pmatrix}. \tag{2.13}$$

In a vacuum, the neutrino mass states are eigenstates of the free particle Hamiltonian

$$\mathcal{H} \left|\nu_k\right\rangle = E_k \left|\nu_k\right\rangle, \tag{2.14}$$

with energy

$$E_k = \sqrt{\mathbf{p}^2 + m_k^2}. \tag{2.15}$$

So the solutions to the time dependent Schrodinger equation are plane waves

$$\left|\nu_k(t)\right\rangle = e^{-iE_k t} \left|\nu_k\right\rangle. \tag{2.16}$$

The time evolution of the initial flavour state is:

$$\left|\nu_\alpha(t)\right\rangle = \sum_k U^*_{\alpha k} e^{-iE_k t} \left|\nu_k\right\rangle. \tag{2.17}$$

The mass states can be written in terms of the flavour states by inverting Equation 2.12:

$$\left|\nu_k\right\rangle = \sum_\alpha U_{\alpha k} \left|\nu_\alpha\right\rangle. \tag{2.18}$$

Here, we have used the fact that the states form an orthonormal basis, $\langle\nu_\alpha|\nu_\beta\rangle = \delta_{\alpha\beta}$, and that the transformation matrix is unitary, $UU^\dagger = \mathbf{1}$.

Substituting Equation 2.18 into the time evolution of the flavour state, Equation 2.17, gives:

$$\left|\nu_\alpha(t)\right\rangle = \sum_{\beta=e,\mu,\tau} \left(\sum_k U^*_{\alpha k} e^{-iE_k t} U_{\beta k} \right) \left|\nu_\beta\right\rangle \tag{2.19}$$

So as the initial flavour state evolves with time, it becomes a superposition of different flavour states; this process is known as neutrino oscillation. The probability of finding the initial neutrino in flavour state ν_β as a function of time is:

$$P_{\nu_\alpha \to \nu_\beta}(t) = |\langle \nu_\beta | \nu_\alpha(t) \rangle|^2 \tag{2.20}$$

$$= \sum_{kj} U^*_{\alpha k} U_{\beta k} U_{\alpha j} U^*_{\beta j} e^{-i(E_k - E_j)t}. \tag{2.21}$$

All neutrino oscillation experiments to date operate in a regime where $E \gg m$, in this regime the relativistic energy relation for neutrinos can be expanded as $E_k \simeq E + \frac{m_k^2}{2E}$, where $E = |p|$. Hence,

$$E_k - E_j \simeq \frac{m_k^2 - m_j^2}{2E} = \frac{\Delta m^2_{kj}}{2E}. \tag{2.22}$$

In addition, neutrino oscillation experiments do not measure the neutrino propagation time t. Instead, they measure the propagation distance, L, also known as the baseline. In the ultra–relativistic limit we can approximate $t \simeq L$ in natural units. As a result, Equation 2.20 can be approximated as:

$$P_{\nu_\alpha \to \nu_\beta}(t) = \sum_{kj} U^*_{\alpha k} U_{\beta k} U_{\alpha j} U^*_{\beta j} e^{-i\frac{\Delta m^2_{kj} L}{2E}}. \tag{2.23}$$

Splitting the sum into its real and imaginary parts emphasises the possibility of CP–violation in neutrino oscillations. CP–violation occurs if the imaginary component of the matrix product is none–zero.

$$P_{\nu_\alpha \to \nu_\beta}(t) = \delta_{\alpha\beta} - 4 \sum_{j>k} \mathrm{Re}(U^*_{\alpha k} U_{\beta k} U_{\alpha j} U^*_{\beta j}) \sin^2\left(\frac{\Delta m^2_{kj} L}{2E}\right)$$

$$\pm 2 \sum_{j>k} \mathrm{Im}(U^*_{\alpha k} U_{\beta k} U_{\alpha j} U^*_{\beta j}) \sin^2\left(\frac{\Delta m^2_{kj} L}{2E}\right). \tag{2.24}$$

The third term here is responsible for CP violation in neutrino oscillations, the positive case corresponds to neutrinos and the negative case is for anti–neutrinos.

The probability of oscillation is therefore dependent on properties determined by nature, in the form of PMNS matrix elements and mass squared differences, and those which can be chosen by experiments, the distance travelled, L, and the neutrino energy, E. In a vacuum, the oscillation probability is only dependent on the

magnitude of the squared mass difference between the neutrino mass eigenstates, it gives no information about the absolute masses of the neutrino eigenstates or their ordering. The question of the absolute neutrino masses cannot be answered in neutrino oscillation experiments, to get access to the absolute masses other experiments are required, e.g. direct mass measurements with tritium beta decay experiments such as KATRIN [**TODO**]. Neutrino oscillation experiments can give insight on the ordering of the neutrino masses, but to understand how the oscillations of neutrinos in matter must be considered.

2.3.1 Neutrino Oscillations in Matter

In real neutrino oscillation experiments, neutrinos travel through matter, whether it be the matter in a star or the earths crust. Neutrinos propagating in matter are subject to an additional potential due to the interaction of the neutrinos with the electrons and nucleons in the medium. This interaction can significantly modify the flavour of the beam relative to oscillations in vacuum.

In matter neutrinos can scatter off particles by interacting with either the charged–current or neutral–current interactions as shown in Figure 2.4. These interactions give rise to additional effective potentials which the neutrinos experience while they are travelling,

$$V_{CC} = \sqrt{2} G_F N_e, \tag{2.25}$$

$$V_{NC}^f = \sqrt{2} G_F N_f g_V^f, \tag{2.26}$$

where G_F is the Fermi weak coupling constant, N_e and N_f are the number densities of electrons and other fermions respectively, and g_V^f is the vector coupling constant for a given fermion f.

Neutral–current scattering is independent of neutrino flavour meaning that the additional potential does not affect oscillations. However, the charged current potential is only present for ν_e, and therefore it will impact the mass eigenstates by different amounts depending on their relative ν_e component.

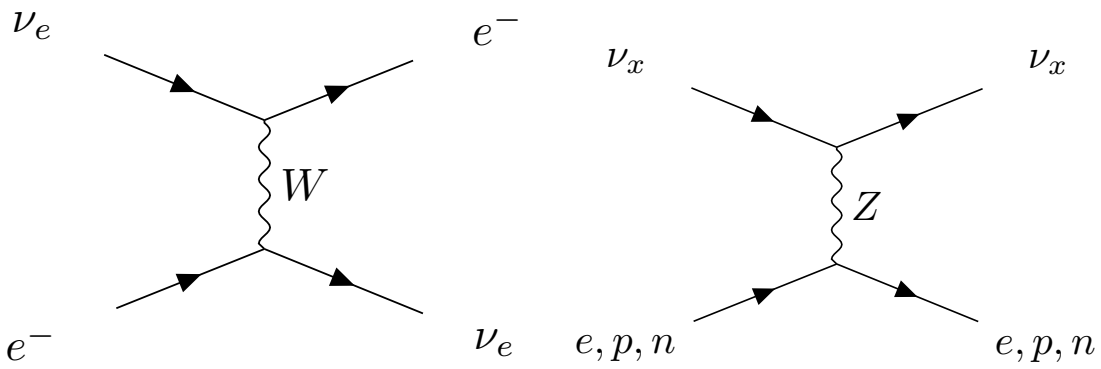

(a) Charged current scattering. **(b)** Neutral current scattering.

Figure 2.4: Feynman diagrams for neutrino scattering in matter.

A full description of the effects of matter on neutrino oscillations is beyond the scope of this thesis, although it is discussed at length in other sources such as [27]. For the purposes of this thesis it is sufficient to note that the propagation of neutrinos in matter changes the oscillations probabilities, and this must be taken into account by oscillation experiments.

One implication of the effects of matter on oscillations is that it introduces sensitivity to sign of the mass splittings [27], allowing experiments to determine the relative ordering of the neutrino masses. By considering the pattern of neutrino oscillations in the Sun it is possible to determine that $\Delta m^2_{21} > 0$ [28]. The sign of the remaining mass splitting, Δm^2_{32}, remains unknown which leaves two possibilities for the ordering of neutrino masses. Normal ordering (NO), in which $m_3 > m_2 > m_1$, and inverted ordering (IO), where $m_1 > m_2 > m_3$, which are depicted in Figure 2.5.

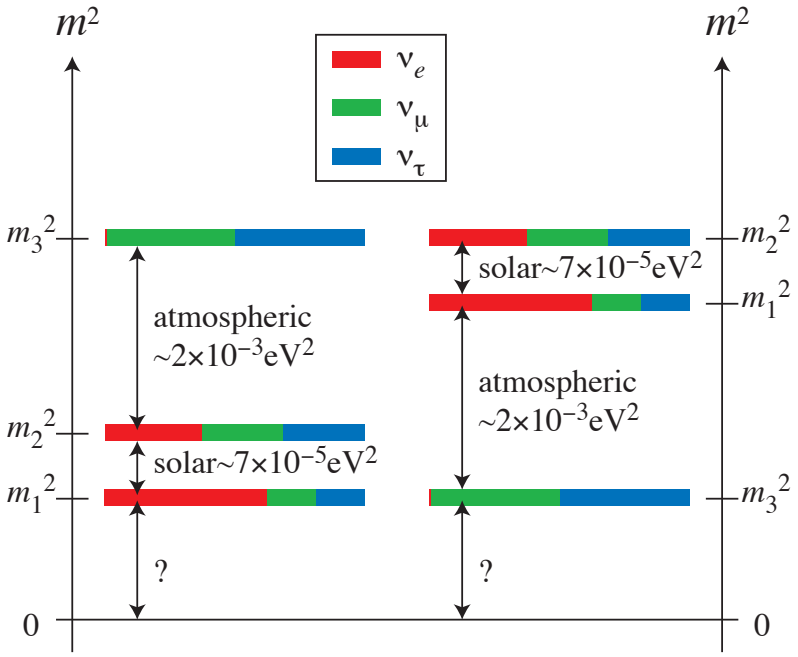

Figure 2.5: The two possible neutrino mass orderings. Left: normal ordering. Right: inverted ordering. Figure from [29].

2.3.2 Current Knowledge and Open Questions

At the time of writing the most widely accepted model of neutrino oscillations involves three neutrino mass eigenstates. In this model, the PMNS matrix is often parametrised in terms of three mixing angles θ_{12}, θ_{13}, and θ_{23} and three CP–violating phases δ_{CP}, α_1, and α_2:

$$U = \underbrace{\begin{pmatrix} c_{12} & s_{12} & 0 \\ -s_{12} & c_{12} & 0 \\ 0 & 0 & 1 \end{pmatrix}}_{\text{Solar}} \underbrace{\begin{pmatrix} c_{13} & 0 & s_{13}e^{-i\delta_{CP}} \\ 0 & 1 & 0 \\ -s_{13}e^{i\delta_{CP}} & 0 & c_{13} \end{pmatrix}}_{\text{Cross–mixing}} \underbrace{\begin{pmatrix} 1 & 0 & 0 \\ 0 & c_{23} & s_{23} \\ 0 & -s_{23} & c_{23} \end{pmatrix}}_{\text{Atmospheric}} \underbrace{\begin{pmatrix} e^{i\frac{\alpha_1}{2}} & 0 & 0 \\ 0 & e^{i\frac{\alpha_2}{2}} & 0 \\ 0 & 0 & 1 \end{pmatrix}}_{\text{Majorana}} . \tag{2.27}$$

Expressing the mixing matrix like this factorises the matrix into its components, which are responsible for oscillations in different regimes. The first component contains only θ_{12} which is dominant in Solar neutrino oscillations. The third component dominates in the mixing of atmospheric neutrinos, and is a function of θ_{23}. The final element which is significant for neutrino oscillations is the second

component, known as the cross–mixing matrix. This component depends on the final mixing angle, θ_{13} and on one of the CP–violating phases, δ_{CP}. If δ_{CP} is non–zero then U will have complex components in off diagonal elements, leading to different probabilities for CP flipped oscillations, $P(\nu_\alpha \rightarrow \nu_\beta) \neq P(\overline{\nu_\alpha} \rightarrow \overline{\nu_\beta})$. Discovery of this effect, which is known as CP–violation, is one of the major goals of the next generation of neutrino oscillation experiments.

The final matrix in the factorised version of the PMNS matrix is called the Majorana component. The CP–violating phases in this matrix cancel in the oscillation probability, and so they can't be measured in neutrino oscillation experiments. In fact, they only lead to physical effects if neutrinos are Majorana particles (i.e. if they are there own antiparticle). Other experiments are required to determine in neutrinos are Majorana particles, for example, neutrinoless double beta decay experiments such as CUORE [30], NEXT [31], and SNO+ [32]. The question of the nature of neutrinos has implications on neutrino mass generation, as mentioned in Equation 2.10.

A large number of neutrino oscillation measurements now exist in the form of solar, reactor, atmospheric, and accelerator neutrino experiments. When combined results from these experiments give us our current best estimates of the neutrino oscillation parameters. The current combined results, from the 2018 Review of Particle Physics by the Particle Data Group [28], along with the major contributing experiments for each measurement are summarised below.

$\boldsymbol{\theta_{12}}$

The constraints on the solar mixing angle θ_{12} are dominated by a combination of data from solar neutrino experiments (e.g. SNO [21] and Super Kamiokande [33]) with data from the KamLAND experiment [24]. The current constraint,

$$\sin^2(\theta_{12}) = 0.297\ ^{+0.017}_{-0.016}, \tag{2.28}$$

comes from a three neutrino fit to the solar and KamLAND data [34].

Δm^2_{21}

The best measurement of Δm^2_{21} comes from the same combined fit to the solar neutrino and KamLAND data [34]. The measured value is

$$\Delta m^2_{21} = (7.37\ ^{+0.17}_{-0.16}) \times 10^{-5}\ \text{eV}^2. \tag{2.29}$$

θ_{23} and Δm^2_{32}

There is a strong correlation between θ_{23} and Δm^2_{32} and therefore their measurements are usually presented as a two–dimensional contour. Figure 2.6 shows a comparison of the world leading contours for $\sin^2(\theta_{23})$–Δm^2_{32}, with the tightest error bands coming from long baseline accelerator experiments such as T2K, MINOS, and NOνA [35–37]. The results are dependent on the neutrino mass ordering, based on a global three neutrino oscillation analysis [34],

$$\begin{aligned} |\Delta m^2_{32}| &= (2.46\ ^{+0.04}_{-0.04}) \times 10^{-3}\ \text{eV}^2 \quad \text{(NO)} \\ &= (2.50\ ^{+0.05}_{-0.04}) \times 10^{-3}\ \text{eV}^2 \quad \text{(IO)}, \end{aligned} \tag{2.30}$$

and

$$\begin{aligned} \sin^2(\theta_{23}) &= 0.437\ ^{+0.033}_{-0.020} \quad \text{(NO)} \\ &= 0.569\ ^{+0.028}_{-0.051} \quad \text{(IO)}. \end{aligned} \tag{2.31}$$

θ_{13}

Reactor neutrino experiments such as Daya Bay [38], Double Chooz [39], and RENO [40] have made the most precise measurements of θ_{13}. A three neutrino global fit to the reactor data gives [34]

$$\sin^2\theta_{13} = (2.15 \pm 0.07) \times 10^{-2}. \tag{2.32}$$

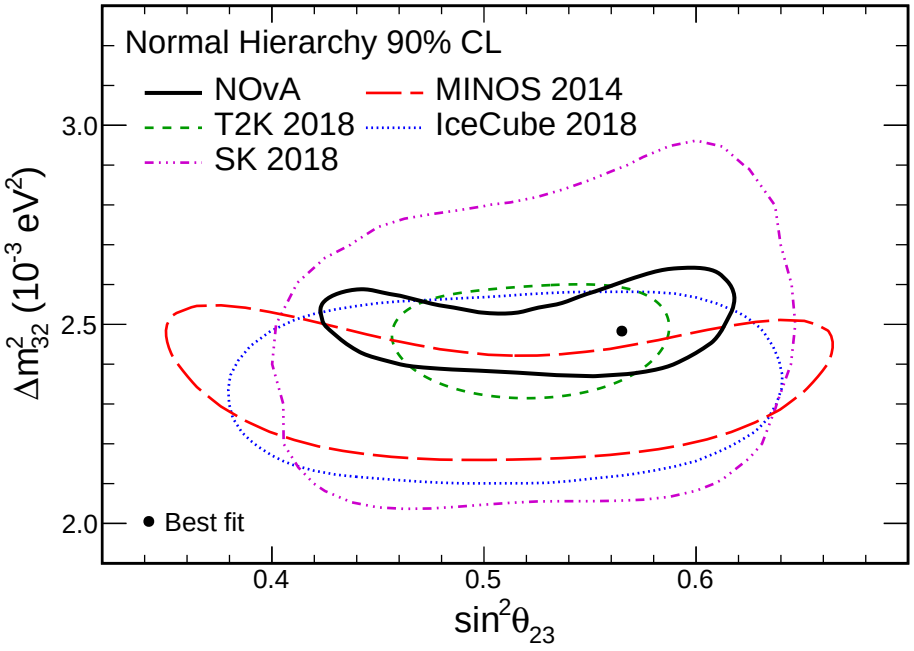

Figure 2.6: The 90% confidence region contours for $\sin^2(\theta_{23})$–Δm^2_{32} from a number of the leading neutrino oscillation experiments [35–37]. The best fit point for the NOνA experiment is shown as a black dot. [37]

δ_{CP}

While there are no accurate measurements of δ_{CP} there are some hints that it may be none–zero from long baseline accelerator neutrino experiments T2K and NOνA.

The T2K experiment's joint fit to electron neutrino appearance and anti–electron neutrino appearance shows an excess of electron neutrino events and a deficit of anti–electron neutrino events when compared to the predictions for $\delta_{CP} = 0$. This results in a preference for negative values of δ_{CP} with a 3σ confidence interval of $[-3.41, -0.03]$ in the case of normal neutrino mass ordering. The results of the T2K fit are shown in Fig. 2.7. [41]

The NOνA experiment has also performed joint fits to neutrino and anti–neutrino oscillation data, the results of the fit are shown in Fig. 2.8. As with T2K the normal mass ordering is preferred, however for NOνA the full range of δ_{CP} is covered at 3σ highlighting the need for further study of CP–violation in neutrino oscillations [37].

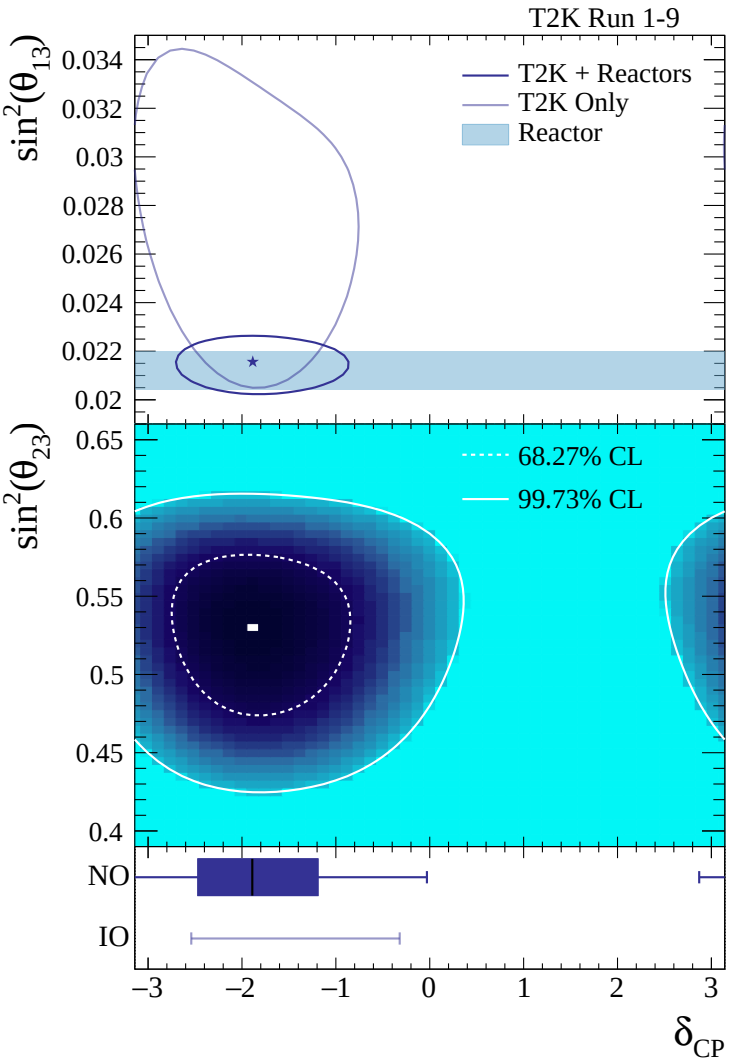

Figure 2.7: Confidence intervals for δ_{CP} from the T2K experiment [41]. Top: 68.27% confidence level contours for δ_{CP} versus $\sin^2\theta_{13}$ under the assumption of normal ordering. Middle : Confidence intervals at the 68.27% and 99.73% confidence level for δ_{CP} versus $sin^2\theta_{23}$ from a fit to T2K and reactor data under the assumption of normal ordering. Bottom: Confidence intervals for δ_{CP} from a fit to T2K and reactor data for both the normal and inverted orderings. The vertical line in the shaded box shows the best-fit value of δ_{CP}, the shaded box shows the 68.27% confidence interval, and the error bar shows the 99.73% confidence interval.

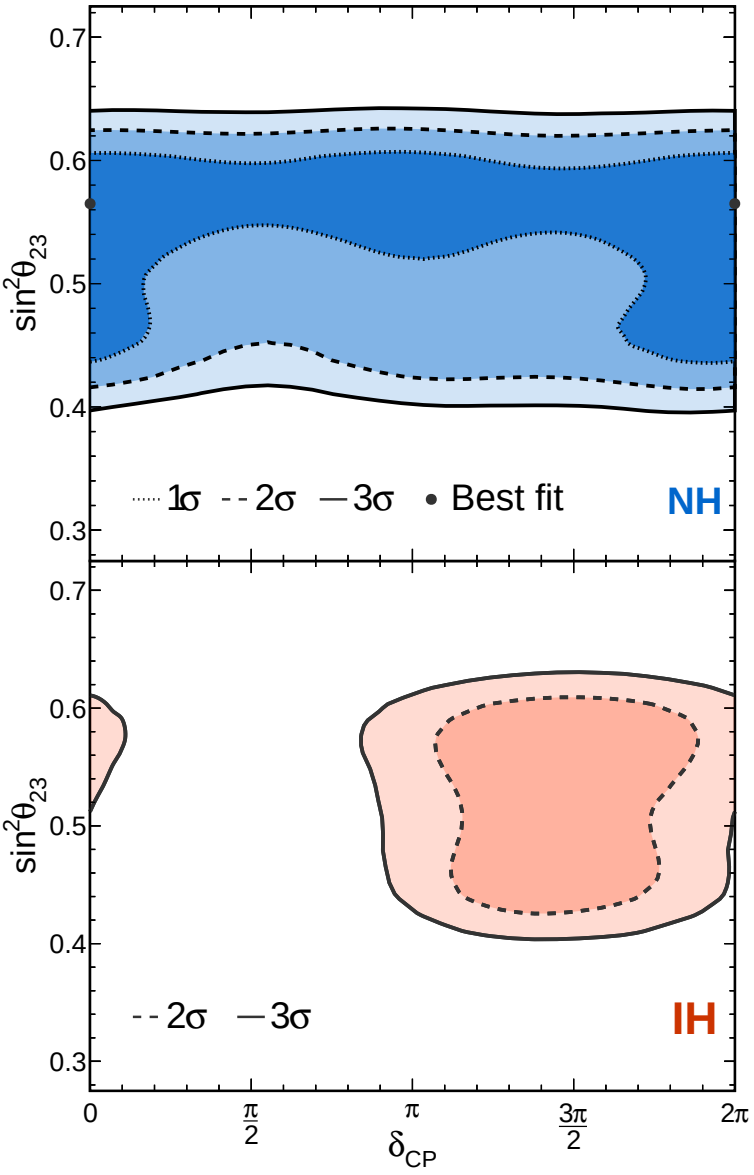

Figure 2.8: Confidence intervals for δ_{CP} from the NOνA experiment [37].
Top: Confidence interval for δ_{CP} versus $\sin^2\theta_{23}$ under the assumption of normal ordering.
Bottom: Confidence interval for δ_{CP} versus $\sin^2\theta_{23}$ under the assumption of inverted ordering.

2.4 Neutrino Interactions

To perform a neutrino oscillation experiment the composition of the beam needs to be measured, and the change in beam composition as a function of energy and distance travelled is analysed. In practice, this relies on measuring neutrino events and categorising them by flavour in order to compare the measurement to prediction. However, because we only see the neutrinos that interact, we are actually seeing the results of a convolution of the neutrino beam composition with the neutrino interaction cross section. Therefore, it is important to understand neutrino interaction cross sections to make accurate oscillation predictions.

Broadly speaking there are two major types of neutrino interactions: charged–current (CC) and neutral–current (NC). Only CC interactions are used in oscillation experiments because they are the only type of interaction which allows the initial flavour of the neutrino to be determined. Some NC interactions, e.g. scattering from an electron, produce high energy leptons in the detector and, therefore, form an irreducible background which must be modelled as part of the experiments simulation.

The types of charged–current interactions available are further split into three main categories.

Quasi–elastic (QE)

A neutrino elastically scatters of an individual nucleon liberating it from the nucleus.

Resonance (RES)

A neutrino excites the target nucleon into a resonance which then decays resulting in the possibility of mesons in the final state.

Deep Inelastic Scattering (DIS)

The neutrino has enough energy to resolve the individual quarks within the target nucleon, liberating the quark and resulting in a hadronic shower in the final state.

The cross sections for these processes vary as a function of neutrino energy, and they are each dominant in different energy regimes. Predictions and measurements

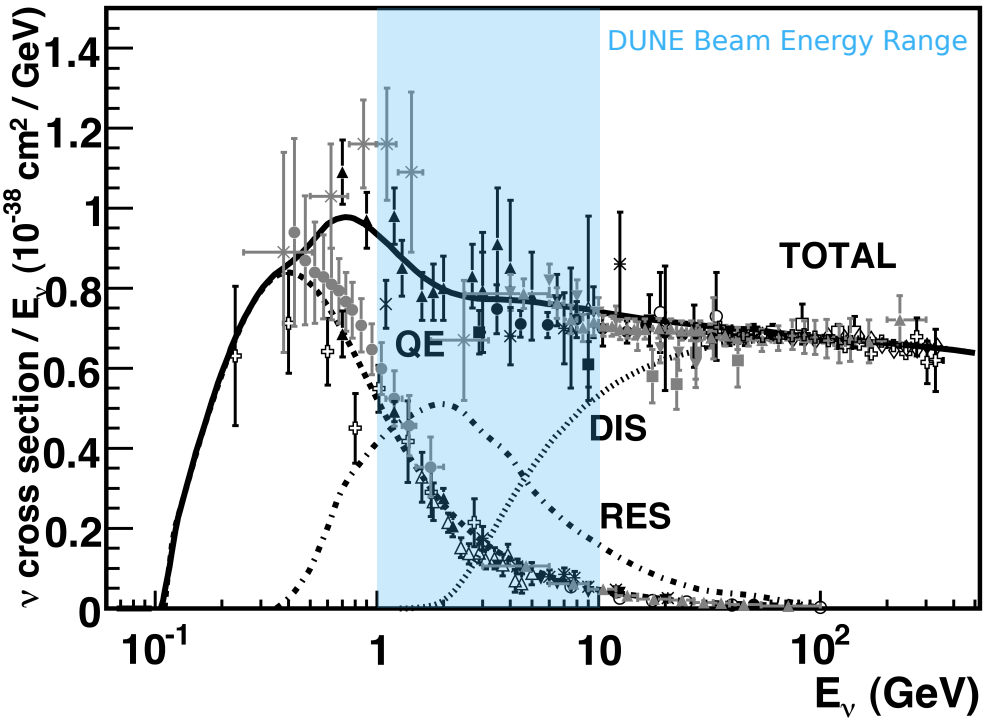

Figure 2.9: Muon neutrino cross section as a function of energy. Original figure from [42].

of the charged–current cross section for ν_μ are shown in Figure 2.9, the three main components of the cross section are shown and the energy range relevant for DUNE is highlighted [42]. Within the energy range of the DUNE beam all three of the major neutrino cross section components have a region in which they dominate, this means that understanding each of these cross sections is crucial for any neutrino oscillation measurement in DUNE.

The array of interaction modes available in DUNE means that there is a wide array particles which can be produced in the final state, and understanding the composition of the final state provides valuable input to the neutrino oscillation analysis. Part of this thesis, Chapter 5, looks at the identification of charge deposits within liquid argon TPCs. The results provide input in the analysis of ProtoDUNE–SP data, and the methods used could be adapted and developed for application in the identification of neutrino interaction modes in DUNE.

2.5 Supernova Neutrinos

Supernovae are extremely violent explosions which are undergone by certain types of stars at the end of their life. These explosions can emit one the order of 10^{53} erg of energy, and in certain cases, known as core–collapse supernovae, about 99% of this energy is carried away by neutrinos. Measurements of these neutrinos can provide insight into the mechanism involved in supernova bursts, as well as the study of neutrino masses [27].

2.5.1 Core–collapse Supernova Dynamics

Core–collapse supernovae occur in stars with masses of around 10–60 solar masses. These stars will have undergone all stages of nuclear fusion during their life, but since iron is the most tightly bond nucleus there is no fuel left to burn after it has been produced. At this stage the iron core of the star, which has a mass of around 1 solar mass, begins to collapse as the pressure produced by nuclear fusion is no longer enough to counter the force of gravity.

During the collapse of the core electron neutrinos are produced through electron capture on both nuclei and free protons.

$$e^- + N(Z, A) \rightarrow N(Z-1, A) + \nu_e \tag{2.33}$$

$$e^- + p \rightarrow n + \nu_e \tag{2.34}$$

At first, the mean free path of these neutrinos is much longer than the size of the core and the neutrinos leave the core carrying away their energy. This phase of the collapse is known as the infall phase, it lasts on the order of 10ms and releases neutrinos with energies of around 12–16 MeV.

Once the density of the core increases beyond around 3×10^{11}g cm^{-3} neutrinos become trapped in the core, as the cross section for coherent scattering becomes large enough to prevent neutrinos from passing through the core. Neutrinos are still being produced by capture processes at this point, but they are unable to leave the core.

The core–collapse comes to a sudden halt about 1 second after it began when the density of the inner core reaches that of nuclear matter. At this stage, the

core settles into equilibrium as a proto–neutron star while a shock–wave caused by this sudden halt propagates out through the layers of the star. Behind the shock, neutrino production is accelerated as nuclei are dissociated and the free protons capture electrons. Neutrinos begin to build–up behind the opaque shock. A few milliseconds after the bounce, the shock reaches a region of low enough density and becomes transparent, releasing the build–up of neutrinos in just a few milliseconds, this is known as the neutronisation burst.

One aspect of supernova dynamics which is still under debate is the so–called revival of the shock. As the shock dissipates through nucleon dissociation and neutrino emission it becomes weakened and eventually stalls around 100 ms after the initial bounce. At this time, known as the accretion phase, matter falls onto the collapsed core. If the shock cannot be revived a supernova will not occur. It is thought that neutrino flux produced in the proto–neutron star is able to revive the shock but the precise mechanics of this revival are still under debate. Studies have shown that the impact of spherically asymmetries might play an important role in allowing the burst to take place [43].

After the neutronisation burst the main remaining source of neutrino production comes from the proto–neutron star. Neutrinos of all flavours are produced in the core at a temperature of around 40 MeV. The release of neutrinos at this stage, known as the neutrino cooling phase, is significantly slower than that of the neutronisation burst and can last tens of seconds. During this phase, much like photons within a star, the neutrinos are mostly contained within the opaque environment of the proto–neutron star. They can only escape if they travel far enough from the core to a region where the opacity is sufficiently low. This region is called the neutrinosphere, it is different for neutrinos of different flavours, and for neutrinos and anti–neutrinos. The difference in the neutrinosphere for each flavour result in different energy distributions for each neutrino type, owing to the relative

temperature of the star at the radius of the neutrinosphere,

$$\langle E_{\nu_e} \rangle \approx 10\text{MeV} \tag{2.35}$$

$$\langle E_{\overline{\nu_e}} \rangle \approx 15\text{MeV} \tag{2.36}$$

$$\langle E_{\nu_x} \rangle \approx 20\text{MeV} \tag{2.37}$$

where $\nu_x \in [\nu_\mu, \overline{\nu_\mu}, \nu_\tau, \overline{\nu_\tau}]$.

2.5.2 SN1987A

The first, and only, experimental observation of neutrinos from a supernova burst occurred in 1987. A small number of low–energy neutrino events where detected in coincidence with a supernova burst from the Large Magellanic Cloud, referred to as SN1987A. Three neutrino detectors reported an excess of low energy events in coincidence with the supernova: Kamiokande–II, IMB, and Baksan. These events are primarily produced by two types of interaction, inverse beta decay (IBD),

$$n + \nu_e \rightarrow p + e^+, \tag{2.38}$$

and elastic scattering,

$$\nu_e + e^- \rightarrow \nu_e + e^-. \tag{2.39}$$

For supernova neutrinos, the inverse beta decay cross section is significantly higher than that of elastic scattering, therefore, most events are likely to be due to inverse beta decay.

2.5.2.1 Kamiokande–II

Kamiokande–II was a water Cerenkov detector containing 2.1 kt of water. A significant increase in the rate of electron events with respect to background was observed in a 10 second window which is coincident with SN1987A [44]. Around 12 events were observed, their time sequence and amplitudes are shown in Figure 2.10. Unfortunately, due to an inaccurate detector clock, the absolute time of these events is only accurate to about one minute and therefore a time coincidence check with the other neutrino observations cannot be made.

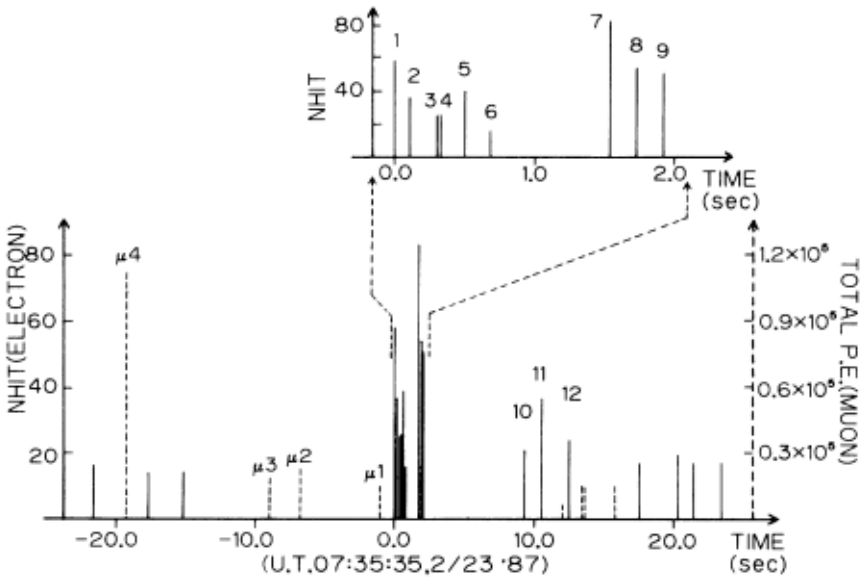

Figure 2.10: Measured supernova neutrino events from SN1987A in Kamiokande–II. Figure from [44].

2.5.2.2 IMB

IMB was another water Cerekov detector, with a fiducial mass of 3.3 kt. They observed eight neutrino candidate events with energies in the range of 20–40 MeV within a six second window, the background rate was estimated to be around 2 events per day [45].

2.5.2.3 Baksan

Unlike Kamiokande–II and IMB, the Baksan detector was a segmented liquid scintillator detector with a total mass of around 330 tons, however only a limited fiducial mass of around 200 tons was used for the supernova neutrino measurements. No excess above background could be observed by Baksan in isolation, however, when assisted by input from Kamiokande–II and IMB, a cluster of 5 events within a 10s window was observed which coincided with the measurements from IMB [46].

Since SN1987A significant progress has been made for both experimental and theoretical aspects of neutrino physics. Progress has been made in modelling supernova explosions, and the impact of neutrino oscillations on the supernova environment have been considered [47]. The current and next generation of neutrino

experiments expect to measure thousands of neutrino events for a galactic supernova instead of tens, this data could provide insights into the dynamics of supernovae as well as neutrino physics.

2.5.3 Supernova Neutrino Prospects in DUNE

The current world leading supernova neutrino detector is Super–Kamiokande which expects to measure around 8000 events for a supernova at 10 kpc [48]. As with Kamiokande–II, these events would primarily be produced via inverse beta decay interactions on the protons within the water. As such Super–Kamiokande is mostly sensitive to the $\overline{\nu_e}$ component of the supernova neutrino flux. This is common amongst all water Cerenkov and scintillator based detectors, and therefore the majority of the current landscape of supernova neutrino detectors. The large charged–current cross section for ν_e on argon therefore makes DUNE a highly complementary detector to the other major supernova neutrino detectors, and DUNE offers a unique sensitivity to the neutronisation burst which is primarily made up of ν_e.

2.5.3.1 Supernova Neutrino Interactions in Liquid Argon

Liquid argon should bring a strong sensitivity to the ν_e component of a supernova neutrino burst, via the charged–current absorption of ν_e on ^{40}Ar,

$$\nu_e + {}^{40}\mathrm{Ar} \rightarrow e^- + {}^{40}\mathrm{K}^*. \tag{2.40}$$

This interaction leaves an e^- and an excited K in the final state. In addition there are charged–current $\overline{\nu_e}$ interactions with argon, and elastic scattering interactions with electrons which are available to neutrinos of all flavours. The dominant cross sections in liquid argon as a function of energy are shown in Figure 2.11 [49].

2.5.3.2 Supernova Neutrino Events in DUNE

For a 10 kpc supernova DUNE expects to observe roughly 3000 neutrino events, over a period of around 10 seconds. In DUNE this will show up as a sudden increase in the rate of low–energy electron events in the detector. Figure 2.12 shows the predicted time structure and energy spectrum for a simulated supernova event in DUNE [49].

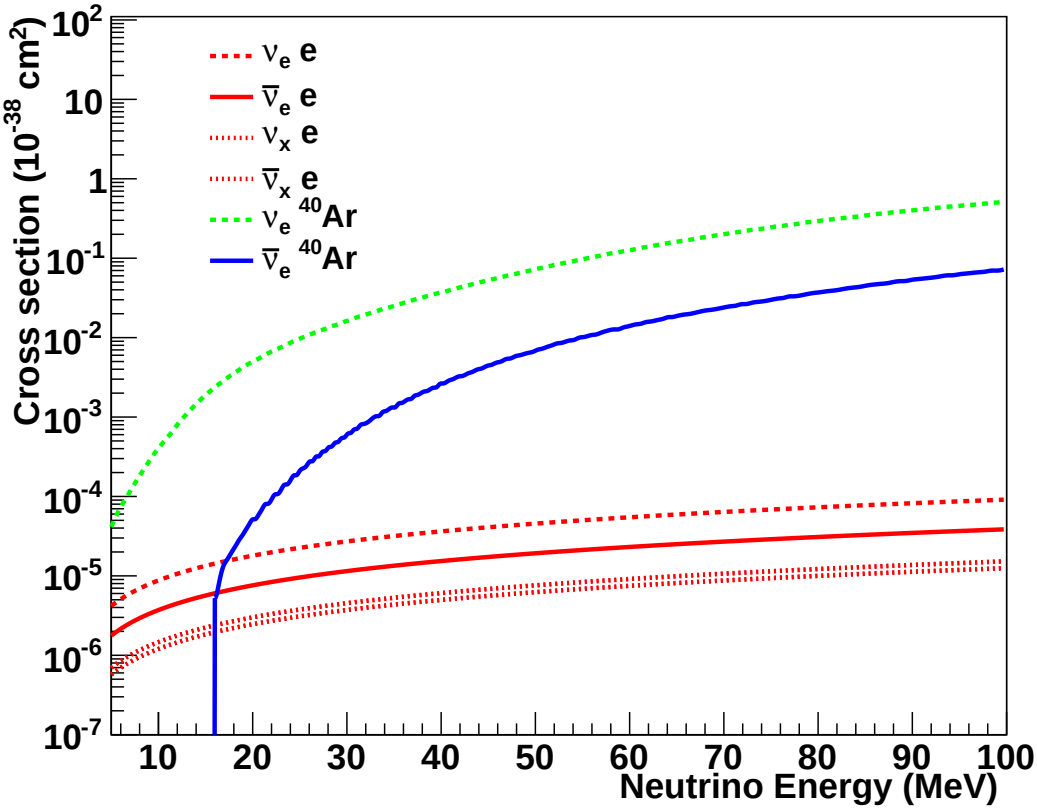

Figure 2.11: Supernova neutrino cross sections in liquid argon. Figure from [49].

The details of the rate and energy of these events as a function of time can hold potential insights into both neutrino physics and the dynamics of supernova bursts.

Detecting and reconstructing tens of MeV electrons from supernova neutrinos is necessary to study supernova neutrinos, as can be seen from the observed energy spectrum for supernova neutrinos in Figure **??**. There are significant challenges involved in this measurement from the detection of low energy activity, as well as the impacts of the ionisation geometry of tens of MeV on reconstruction. Effectively reconstructing electrons in the tens of MeV range is essential to improving our understanding of supernova neutrinos in DUNE. This is one of the subjects of this thesis, and is discussed in chapter 6 using the case of Michel electrons in ProtoDUNE–SP to benchmark the performance of low energy electron reconstruction in liquid argon time projection chambers.

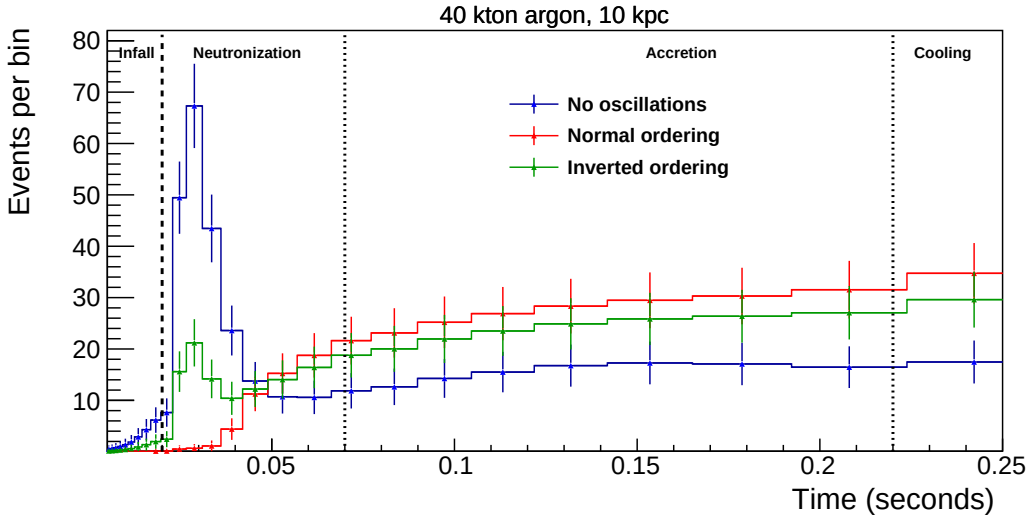

(a) Observed event rate. Figure from [49].

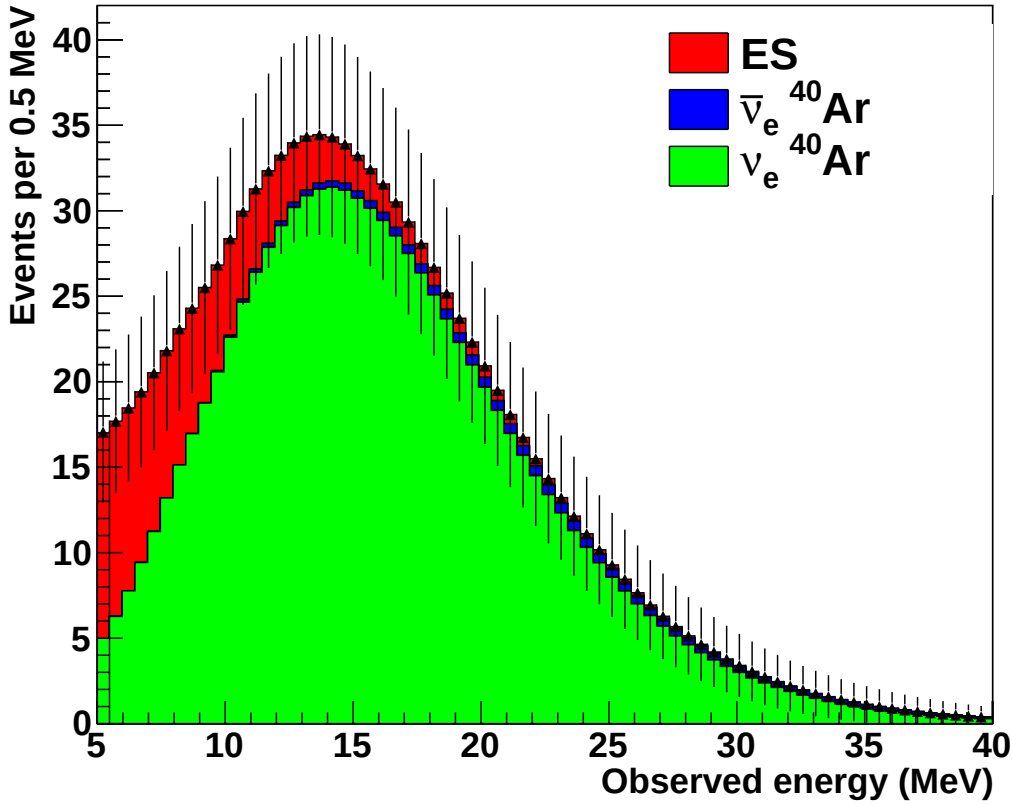

(b) Observed energy. Figure from [50].

Figure 2.12: Supernova neutrinos predictions for a 10kpc supernova in DUNE.